

# Anomalous pinch in electron-electron beam collision

W. Zhang,<sup>1,2,\*</sup> T. Grismayer,<sup>3,†</sup> and L. O. Silva<sup>3,‡</sup>

<sup>1</sup>*Jiangxi Province Key Laboratory of Nuclear Physics and Technology,  
East China University of Technology, Nanchang 330013, China*

<sup>2</sup>*Engineering Research Center of Nuclear Technology Application,*

*Ministry of Education, East China University of Technology, Nanchang 330013, China*

<sup>3</sup>*GoLP/Instituto de Plasmas e Fusão Nuclear, Instituto Superior Técnico, Universidade de Lisboa, Lisboa, Portugal*

(Dated: December 13, 2024)

We show that an anomalous pinch can occur in ultrarelativistic electron-electron or positron-positron beam interaction, caused by the combined interplay of collective beam motion (disruption) and strong-field quantum electrodynamics (SF-QED). The locally created electron-positron pairs, from SF-QED effects, screen the self-fields of the beams and can invert the polarity of the Lorentz force resulting in a pinch of the beams. A theoretical model predicts the pinch condition and is confirmed by first-principles 3-dimensional particle-in-cell simulations. This anomalous pinch enhances density compression, increases the collision luminosity, and amplifies the local magnetic fields and the quantum parameter of the beam particles by several orders of magnitude.

Advanced lepton (electron  $e^-$  and positron  $e^+$ ) accelerators are indispensable tools for a wealth of disciplines including the frontier particle physics [1–5]. The collisions between ultrarelativistic and dense lepton beams have been proposed as a platform for studying the strong field quantum electrodynamics (SF-QED) [6–9], including the non-perturbative regime [7]. These collision studies are important to the Interaction Point (IP) dynamics of high-energy physics experiments [10], because the collective processes of the beams can deteriorate the beams and produce secondary particles that might hinder the outcome of the experiments. For dense beams ( $n > 10^{23} \text{ cm}^{-3}$ ) the particles are subject to the intense electromagnetic fields ( $E/E_s > 10^{-4}$  with  $E_s$  the Schwinger field) of the oncoming beam, leading to beamstrahlung [11, 12] and  $e^-e^+$  pair creation [13]. In addition, the beams can also be subject to disruption, i.e., the collective transverse motion of the beams [14], quantified by the parameter

$$D = \eta \frac{N_0 r_e \sigma_z}{\gamma \sigma_0^2} = \frac{3}{2} \eta \frac{N_0 [10^{10}] \sigma_z [\mu\text{m}]}{\mathcal{E}_0 [\text{GeV}] (\sigma_0 [0.1 \mu\text{m}])^2}, \quad (1)$$

where  $N_0$  is the number of particles,  $r_e = e^2/mc^2$  the classical electron radius (with the usual definition of the electron charge, mass, and the speed of light),  $\mathcal{E}_0 = \gamma mc^2$  with  $\gamma$  the Lorentz factor,  $\sigma_0$  and  $\sigma_z$  the transverse width and longitudinal length, respectively. Disruption becomes dynamically significant when  $D \geq 1$  with  $\eta$  depending on the beam profile: 4 for a uniform beam and 1 for a Gaussian beam [6]. Disruption leads to oscillations of the beams around the propagation axis in collisions of opposite-charge ( $e^-e^+$ ) beams, and defocusing of beams in identical-charge ( $e^-e^-$  or  $e^+e^+$ ) collisions. Previous studies on SF-QED effects in lepton collisions considered the limit of negligible disruption [6–9]. This assumption becomes no longer valid for collisions in future colliders, where the beams possess  $\mu\text{m}$ -scale length and  $\text{nm}$ -scale width [15, 16] with  $D \gg 1$  and the quantum param-

eter  $\chi = \sqrt{(\gamma \mathbf{E} + \mathbf{p}/mc \times \mathbf{B})^2 - (\mathbf{p}/mc \cdot \mathbf{E})^2}/E_s$  larger than unity [8] where  $\mathbf{E}, \mathbf{B}$  are the electromagnetic fields,  $E_s = m^2 c^3 / e \hbar$ ,  $\hbar$  is the reduced Planck constant, and  $\mathbf{p}$  is the particle's momentum. The disruption will affect the beam profiles and fields, altering the SF-QED rates. It was shown that even a mild disruption ( $D \sim 1$ ) in  $e^-e^-$  collisions would reduce the beamstrahlung [8] as compared to  $D \ll 1$ . This is due to the dilution of the beams which causes a decrease in the fields. The SF-QED processes can affect the disruption dynamics [8, 17]. However, the effect of copious pair production expected when  $\chi \gg 1$  and  $D \gg 1$  has not been investigated. As we show in this Letter, the pairs screen the self-fields of the beams and can invert the polarity of the Lorentz force. This force inversion leads to the anomalous pinch (AP) in the collision of identical-charge beams ( $e^-e^-$  or  $e^+e^+$ ). The focusing effect of the created positrons has been observed in CAIN simulations for the design of a Collider Higgs Factory [18]. AP is not a single isolated phenomenon; it belongs to the class of scenarios where the density of produced pairs becomes high enough to alter the background fields. In laser-electron scattering, it leads to frequency up-shifts [19, 20], and in laser-driven QED cascades, to significant laser absorption [21, 22], whereas, in neutron-star-associated cascades, it triggers the emission of plasma waves [23–25].

We consider  $e^-e^-$  collisions whose setup is sketched in Fig. 1. The beams are assumed to be cold, cylinder-shaped, with uniform density  $n_0$  with initial profiles  $n_j = n_0$  ( $j = 1, 2$ ) for  $r \leq \sigma_0$ ,  $-\sigma_z \leq z_j \leq 0$ . The unexplored regime  $D \gg 1$  and  $\chi \gg 1$  implies the time scale hierarchy:  $\tau_{col} \gg \tau_D \sim \tau_{QED}$ , where  $\tau_{col} = \sigma_z/c$  is the collision time,  $\tau_D = D^{-1/2} \tau_{col}$  is the characteristic disruption time, and  $\tau_{QED} (\propto \chi^{-2/3})$  is the typical photon emission or photon decay time (which are on the same order when  $\chi \gg 1$ ) [26–28]. The pairs are created on the  $\tau_{QED}$  time scale before the beams have been disrupted. The separation of scales allows the estimate of the dilu-

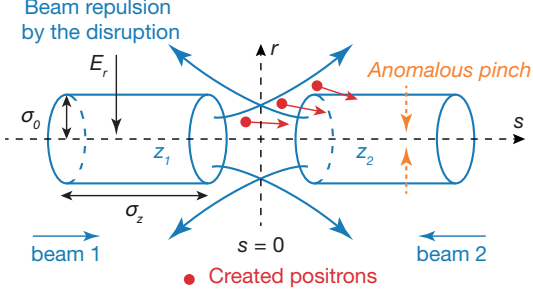


FIG. 1. (Color online). Schematic of the collision. The colliding (electron) beams are labeled as beam 1 and beam 2. The coordinate  $s$  [14] represents the longitudinal coordinates fixed in the center-of-mass frame.  $z_j$  ( $j = 1, 2$ ) denotes the longitudinal position co-moving with the two beams. The slice at  $z_1$  of beam 1 will meet the slice at  $z_2$  of beam 2, at the location  $s$  and time  $t$  which are bound by  $s = z_1 + ct = -z_2 - ct$ .

tion of beams and the density of created pairs with the undisrupted beam self-fields ( $E_{r,0} = -2\pi en_0 r$  for  $r \leq \sigma_0$  and  $-2\pi en_0 \sigma_0^2/r$  for  $r > \sigma_0$ , the strength of azimuthal magnetic field satisfies  $|B_{\theta,0}| \simeq |E_{r,0}|$  [8]).

*Beam dilution.* When beamstrahlung is discarded, the particle energy can be assumed constant during the collision. The equation of motion, under the undisrupted fields, for  $r < \sigma_0$  is  $d^2 r/dt^2 = (\omega_b^2/\gamma)r$ , and for  $r > \sigma_0$  is  $d^2 r/dt^2 = (\omega_b^2/\gamma)(\sigma_0^2/r)$ , where  $\omega_b = \sqrt{4\pi e^2 n_0/m}$  is the beam plasma frequency. The trajectory of an electron that stays within the beam, at  $z_j$  with initial position  $r_{0,j}$ , is given by  $r_j(z_j, t) = r_{0,j} \cosh(\Delta t_j/\tau_D)$ . Here,  $\tau_D = \sqrt{\gamma}/\omega_b$ ,  $\Delta t_j = t - t_{0,j}$ , and  $t_{0,j} = -z_j/2c$  is the time when the electron crosses the front of the other beam. This trajectory solution indicates that particles are blown away, as sketched in Fig. 1 and that a beam slice expands at a time scale  $\tau_D$ . For short times  $t < \tau_D$ , we can expand the trajectory solution and obtain  $r_j(z_j, t) \simeq r_{0,j}[1 + \frac{1}{2}D(\Delta t_j/\tau_{col})^2]$ . With the equation of continuity  $ndr^2 = n_0 dr_0^2$ , the beam densities read

$$n_{1,2}(s, t) = \frac{n_0}{\left[1 + \frac{1}{2}D(\Delta t_{1,2}/\tau_{col})^2\right]^2}, \quad (2)$$

with  $\Delta t_{1,2} = \frac{1}{2}(t \pm \frac{s}{c})$ ,  $ct - \sigma_z \leq s \leq ct$  for beam 1, and  $-ct \leq s \leq \sigma_z - ct$  for beam 2.

*Pair creation.* Photon emission and pair creation in the SF-QED regime [26–29] are characterized by the quantum parameter  $\chi$ . In beam-beam collisions, the electron quantum parameter is  $\chi_e(r) = (r/\sigma_0)\chi_{e \max}$ , where  $\chi_{e \max} = 4\pi e\gamma n_0 \sigma_0/E_s$ . When the two beams start colliding, pair production follows an SF-QED shower behavior because the particle trajectories remain almost perpendicular to the self-fields. Before the onset of disruption, and for  $\chi$  up to a few 10's, only the first generation of pairs is relevant [30, 31]. If the radiation cooling of the

electron beam is discarded, the density of pairs is [30]

$$n_p(r, t) = n_0 \int_0^t dt' \int_0^{\chi_e(r)} d\chi_\gamma \frac{d^2 W}{dtd\chi_\gamma} \left[1 - e^{-W_p(\chi_\gamma)(t-t')}\right], \quad (3)$$

where  $d^2 W/dtd\chi_\gamma$  is the differential probability rate of photon emission [8],  $\chi_\gamma = \xi\chi_e$  is the quantum parameter for photons, and  $\xi = \mathcal{E}_\gamma/\mathcal{E}_0$  the normalized photon energy.  $W_p(\chi_\gamma)$  is the rate of pair creation from a photon with  $\chi_\gamma$  [26]. In the hierarchy of time scales previously assumed,  $n_p(r, t) \simeq n_0 \mathcal{R}^2(r)t^2/2$ , where  $\mathcal{R}^2(r) = \int_0^{\chi_e(r)} d\chi_\gamma (d^2 W/dtd\chi_\gamma) W_p(\chi_\gamma)$ . In the limit  $\chi_e \gg 1$ ,  $\mathcal{R}(r) \simeq \sqrt{\ln \chi_e(r)} \chi_e^{-1/3}(r) W_\gamma(r)$ , where  $W_\gamma(r) = \int_0^{\chi_e(r)} d\chi_\gamma d^2 W/dtd\chi_\gamma \simeq 1.46\alpha/(\tau_c \gamma) \chi_e^{2/3}$  [26] with  $\tau_c = \hbar/mc^2$  the Compton time and  $\alpha$  the fine-structure constant.

The new electrons are expelled from the initial beam region whereas the positrons remain confined (the opposite in a  $e^+e^+$  collision). The increasing positron population will first screen the self-fields of the beams and then invert the polarity of the Lorentz force. This inversion causes a pinch of the beam electrons, more pronounced in the middle and tail parts, as sketched in Fig 1. The pinch can be quantified using our previous results. At the front of beam 1 (with  $s = ct$ ), the expelling force exerted on beam 2 is  $F(r, t) = 4\pi e^2 n_e(t)r$ , where  $n_e(t) = n_0[1 + D(t/\tau_{col})^2/2]^{-2}$ . Suppose the charge separation of new electrons and positrons occurs almost instantaneously. In that case, the focusing force, from the positrons and experienced by beam 2, is  $F_p(r, t) = -2eE_p(r, t)$ , where  $E_p(r, t) = 4\pi e \int_{r_0}^r n_p(r', t)r'dr'/r$  and  $r_0 = \sigma_0/\chi_{e \max}$ . The focusing force is given by

$$F_p(\sigma_0, t) \simeq -\frac{3\pi}{2}e^2 n_0 \sigma_0 \mathcal{R}^2(\sigma_0)t^2. \quad (4)$$

The pinch can occur if the polarity of the total force is inverted, i.e.,  $F_{tot} = F(\sigma_0, t) + F_p(\sigma_0, t) < 0$ . The time  $t_F$  corresponding to  $F_{tot} = 0$  is obtained by solving  $\frac{3}{8}\mathcal{R}^2(\sigma_0)t_F^2 \left[1 + \frac{1}{2}D\frac{t_F^2}{\tau_{col}^2}\right]^2 = 1$ :

$$\frac{t_F}{\tau_{col}} \simeq \frac{1}{\sqrt{2D}} \left( \sqrt{1 + \frac{32D}{3\mathcal{R}^2(\sigma_0)\tau_{col}^2}} - 1 \right)^{1/2}. \quad (5)$$

At  $t_F$ , the positron density is  $n_p/n_0 = (4/3)[1 + D(t_F/\tau_{col})^2/2]^{-2} \leq 1$ , and in the limit of high disruption ( $D \gg 1$ ),  $t_F \rightarrow \sqrt{32/6D}^{-1/4} \mathcal{R}(\sigma_0)^{-1} \sim \tau_{QED} \sim W_\gamma^{-1}$ .

The charge separation of the created electrons and positrons occurs on the typical disruption time ( $\tau_D$ ), as observed in mild-disruption collisions ( $D \sim 1$ ) in a previous study [8]. The onset of the pinch (characterized by  $t_{AP}$ ) should be bounded as  $t_F < t_{AP} \lesssim t_F + \tau_D$ . Our numerical study shows that notable pinching is observed when  $t_{AP} \lesssim \tau_{col}/2$  which implies  $t_F + \tau_D \leq \tau_{col}/2$ . For  $D \gg 1$ , this criterion for pinch formation can be recast

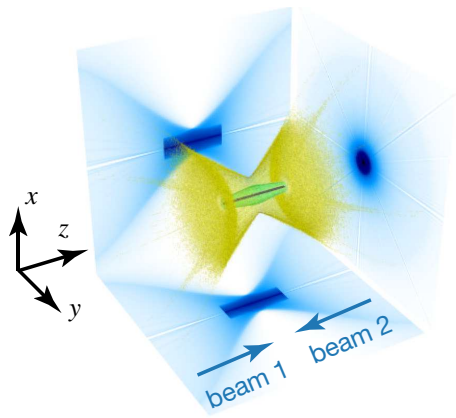


FIG. 2. (Color online). Anomalous pinch in a 3D PIC simulation of an electron-electron collision. The colors represent different iso-density contours. The yellow region ( $n/n_0 = 0.1$ ) shows the expanding fronts of the beams. The green ( $n/n_0 = 1$ ) and purple ( $n/n_0 = 10$ ) regions show the core layers of the pinched beams. The beam parameters are:  $\mathcal{E}_0 = 70$  GeV,  $\sigma_z = 12 \mu\text{m}$ ,  $\sigma_0 = 4.9$  nm, and  $N_0 = 1.3 \times 10^9$ , corresponding to  $D = 54$  and  $\chi_{e\text{max}} = 13$ .

as  $\mathcal{E}_0[\text{GeV}]/\sigma_z[\mu\text{m}] \leq 5D^{1/4}\chi_{e\text{max}}^{1/3}$  which can be further translated into a convenient form as

$$\frac{(\mathcal{E}_0[\text{GeV}])^{11/12} (\sigma_0[0.1\mu\text{m}])^{5/6}}{(\sigma_z[\mu\text{m}])^{11/12} (N_0[10^{10}])^{7/12}} \leq 7. \quad (6)$$

### 3-Dimensional (3D) particle-in-cell (PIC) simulations.

The pinch has been investigated by 3D PIC simulations using OSIRIS [32] where the SF-QED effects are self-consistently included (see Supplemental Material [33]). Figure 2 shows a typical collision between cylinder-shaped electron beams including all the relevant physics. The theoretical criterion for the AP formation [Eqs. (5) and (6)] has been verified by PIC simulations where we have measured the times  $t_{\text{AP}}$  when the total transverse force vanishes in the different simulations (Fig. 3). For  $\sigma_z = 6 \mu\text{m}$ ,  $t_{\text{AP}}$  seems slightly above the curve  $t_F + \tau_D$ , whereas for  $\sigma_z = 12 \mu\text{m}$ ,  $t_{\text{AP}}$  confirms the analytical results and lays between  $t_F$  and  $t_F + \tau_D$ . Even if the total force has vanished or switched polarity a significant electron pinch is only observed for the points under  $\tau_{\text{col}}/2$ . This shows that high disruptions (large  $D$ ) with elongated beams (large  $\sigma_z$ ) are required for driving the pinch at an early stage of the collision, such that the pinch has enough time to develop to become noticeable. When both  $D$  and  $\sigma_z$  are chosen such that  $t_{\text{AP}} > \tau_{\text{col}}/2$ , the AP is too weak to impact the collision dynamics.

*Impact of AP on the luminosity.* This pinch also has consequences on the main beam parameters of the IP. The collision luminosity is  $L_0 = 2c \int \int \int \int n_1 n_2 dx dy dz dt$  [34]. It represents the total number of scattering events at the IP. When the disruption is negligible ( $D \ll 1$ ),  $L_0$  is the geometric luminosity ( $L_0 = L_0^{G_{eo}}$ ), and for cylinder-shaped and uniform beams,  $L_0^{G_{eo}} = N_0^2/\pi\sigma_0^2 = \pi n_0^2 \sigma_0^2 \sigma_z^2$ .

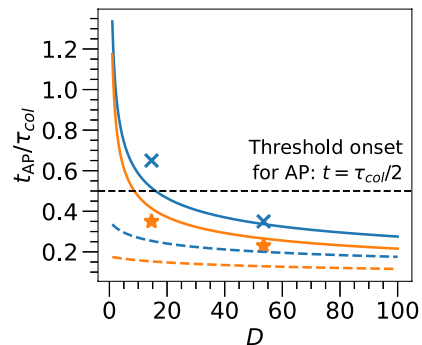


FIG. 3. (Color online). Onset time of AP ( $t_{\text{AP}}$ ) as a function of the disruption parameter for different beam lengths, measured from PIC simulations (symbols) and compared with theoretical predictions and the typical threshold formation time ( $t = \tau_{\text{col}}/2$ ). The simulations are performed for  $D = 14.6$  and  $54$ , respectively. The blue and orange colors are for  $\sigma_z = 6 \mu\text{m}$  and  $12 \mu\text{m}$ , respectively. We maintain  $\mathcal{E}_0 = 70$  GeV, and choose the density  $n_0$  and waist  $\sigma_0$  to keep  $\chi_{e\text{max}} = 13$  constant. The dashed lines depict  $t_F/\tau_{\text{col}}$  [Eq. (5)], and solid lines represent  $(t_F + \tau_D)/\tau_{\text{col}}$ . The simulations verify that significant AP occurs in the early stage of collisions (with  $t_{\text{AP}} < \tau_{\text{col}}/2$ ), and  $t_{\text{AP}}$  lays between  $t_F$  and  $t_F + \tau_D$  in agreement with our model.

For significant disruption and neglecting the SF-QED, the luminosity of  $e^-e^-$  collisions is reduced by the factor  $H_D = L_0/L_0^{G_{eo}}$  that can be calculated for mild and large disruptions. There are two ways of looking at the expansion  $t < \tau_D$  that leads to Eq. (2). The expansion is valid for short times for all  $D$  or during the whole collision time but for mild  $D$ . With a cylindrical dilution, the expression of the luminosity reduces to  $L_0 = 4L_0^{G_{eo}} \int dt \int ds \int n(s,t)/n_0$ . For mild disruptions, the dilution is given by Eq. (2), which gives  $H_D = 8/(8 + D)$ . When  $D \gg 1$  (with  $\tau_D \ll \tau_{\text{col}}$ ), the electrons will move beyond the initial volume of the beams for longer times, and then experience the vacuum fields. The asymptotic particle trajectory for  $t \gg \tau_D$  is  $r_j(z_j, t) \simeq r_{0,j} [1 + \sqrt{D}/2(\Delta t_j/\tau_{\text{col}})]$ . We can similarly compute the density dilution for  $D \gg 1$  and we obtain  $H_D$  as

$$H_D \simeq \frac{32}{D} \left[ \ln\left(1 + \frac{\sqrt{D}}{4}\right) - \frac{\sqrt{D}}{\sqrt{D} + 4} \right]. \quad (7)$$

Figure 4(a) shows that the theoretical predictions of  $H_D$  are in excellent agreement with the QED-free PIC simulations. When SF-QED is included (blue stars), the slower decrease of  $H_D$  is a manifestation of the AP. When  $D$  is mild (for  $D = 14$ ) the onset of the AP occurs close to  $t \simeq \tau_{\text{col}}/2$  (see Fig. 3) and the beams cannot be pinched efficiently resulting in a  $H_D$  similar to the QED-free result. For  $D \gg 10$ ,  $H_D$  becomes significantly enhanced by AP. We have also compared OSIRIS results with GUINEA-PIG [35] for Gaussian beams and

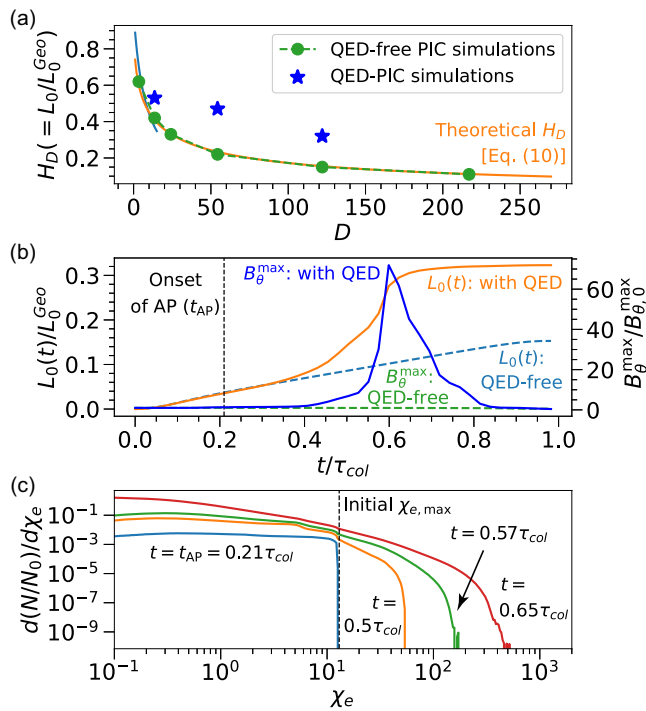


FIG. 4. (Color online). (a) Luminosity reduction  $H_D$  for  $e^-e^-$  collisions as a function of the disruption parameter. The solid lines represent the theoretical models. For the mild- $D$  regime (light blue),  $H_D = 8/(8 + D)$ ; for the high- $D$  regime (orange),  $H_D$  is given by Eq. (7). The 3D simulations with SF-QED switched off show an excellent agreement with the models. These simulations use cylinder-shaped beams with different  $\sigma_z$  while keeping other parameters unchanged, including  $\mathcal{E}_0 = 70$  GeV,  $\sigma_0 = 11.3$  nm, and  $n_0 = 6.23 \times 10^{23}$  cm<sup>-3</sup>. (b) PIC simulations for an  $e^-e^-$  collision with  $\sigma_z = 27.6$   $\mu$ m,  $D = 122$ , and  $\chi_{e,max} = 13$ . The other parameters, including  $\mathcal{E}_0$ ,  $\sigma_0$ , and  $n_0$ , are the same with (a). Left axis: the luminosity growth over time ( $L_0(t)/L_0^{Geo}$ ). Right axis: the maximum magnetic field ( $B_{\theta}^{max}/B_{\theta,0}^{max}$ , with  $B_{\theta,0}^{max}$  the initial peak field). The measured AP onset ( $t_{AP} = 0.21\tau_{col}$ ) is indicated. (c) Evolution of the  $d(N/N_0)/d\chi_e$  distribution in the collision shown in (b). One observes that the distribution develops a tail pushed into the deep-quantum regime by AP.

obtained excellent agreement without SF-QED and reasonable agreement with SF-QED (see Supplemental Material [33]). We want to stress that these results are obtained with perfectly collimated beams corresponding to zero emittance, to compare directly with our theory. We have also conducted the same QED-PIC simulations with finite-emittance beams (divergence angle  $\theta \sim$  mrad or normalized emittance  $\epsilon_n \sim$  mm mrad) without significant differences compared with the zero-emittance results ( $\sim 10\%$  difference). The zero-emittance predictions remain valid when the thermal divergence is smaller than the disruption-induced deflection [6, 8], i.e.,  $\theta < D\sigma_0/\sigma_z$ . This is verified for the regime here with  $D \gg 1$  and typical beam dimension of  $\sigma_z \sim 10$   $\mu$ m and  $\sigma_0 \gtrsim 10$  nm.

The enhancement of the factor  $H_D$  is a direct consequence of the increase of the instantaneous luminosity when AP occurs, as shown in Fig. 4(b). The onset of the pinch is observed around  $t \simeq 0.2\tau_{col}$  in agreement with the theoretical estimate ( $t_F + \tau_D$ ). The luminosity with QED effects departs from  $L_0(t)$  shortly after the AP onset and rises until  $t \simeq 0.6\tau_{col}$ , the pinch stage of the tail of the electron beams. Nevertheless, the pinch cannot go indefinitely because beam instabilities mediated by QED effects [17, 36] will eventually compete with the compression and destroy the beams. These instabilities such as kink or hose have a typical growth rate of  $\omega_b/\sqrt{\gamma} = 1/\tau_D$  [37]. Even without a thorough study, we can conjecture that this limits the compression stage to a few  $\tau_D$ . The saturation of the luminosity (flattening of the orange curve) for  $t > 0.6\tau_{col}$  conveys the emergence of these beam instabilities, that we have observed in our simulations.

*Discussion and Conclusion.* We showed that the interplay between high disruption and SF-QED effects in ultrarelativistic  $e^-e^-$  collisions results in a surprising modification of the collective beam dynamics. The SF-QED shower of positrons can reach a density capable of screening the self-fields and inverting the initially repelling Lorentz force acting on the electrons, eventually leading to an anomalous pinch of the beam. The pinch can be efficient for sufficiently long ( $\sigma_z > 10$ 's  $\mu$ m), and thin ( $\sigma_0 > 10$ 's nm) beams. The anomalous pinch represents a tangible manifestation of the back-reaction of pair creation on the self-fields of the beams. Whereas the pinch might not be directly observed in an experiment, the outcome of the scattering events determined by the luminosity would be enhanced by the pinch of the beams.

Additional fundamental and exotic phenomena associated with the pinch are relevant to future works. As the beam is being compressed, the self-fields of the beam are also increased, as shown in Fig. 4(b). This effect of strong self-field amplification and density compression was first described in  $e^-e^+$  collisions in [38]. Using particle conservation, the pinched density scales as  $1/\sigma_0^2(t)$  with the beam waist  $\sigma_0(t)$  decreasing during AP. The associated electromagnetic fields and the quantum parameter are enhanced as  $1/\sigma_0(t)$ . Therefore, the AP can be used to access the frontier of the non-perturbative SF-QED regime [7] for fundamental studies. As an example, the peak of the magnetic field is increased by more than 70 times in the pinching areas of the collision as shown in Fig. 4(b). For the beam electrons that have not suffered radiation loss, their  $\chi_e$  are raised by the same magnetic field compression factor showing  $\chi_e \gtrsim 500$ . This  $\chi_e$  amplification is illustrated in Fig. 4(c) which displays the  $\chi_e$  distribution at four times, allowing to approach the non-perturbative SF-QED with state-of-the-art electron beams.

We want to acknowledge discussions with Dr. D. Del Sorbo, Professor F. Fiuza, Professor W. Mori, Dr. Tim

Barklow, and Dr. Glen White. This work was supported by FCT (Portugal) Grants No. 2022.02230.PTDC (X-MASER), UIDB/FIS/50010/2020 - PESTB 2020-23, Grants No. CEECIND/04050/2021 and PTDC/FIS-PLA/ 3800/2021. W.Z. is supported by Jiangxi Provincial Natural Science Foundation (the Young Scientists Fund, No. 20242BAB21003) and the Start-up Fund (No. DHBK2023009) from East China University of Technology (Nanchang, China). We acknowledge EuroHPC for awarding access to Karolina supercomputer in Czech Republic and MareNostrum at Barcelona Supercomputing Center (BSC, Spain). Simulations were performed at National Supercomputer Center in Guangzhou (China), Karolina (Czech Republic), and MareNostrum (Spain).

\* wenlong.zhang@ecut.edu.cn

† thomas.grismayer@tecnico.ulisboa.pt

‡ luis.silva@tecnico.ulisboa.pt

- [1] J. Ellis, “The future of high-energy collider physics,” (2018), arXiv:1810.11263 [hep-ph].
- [2] V. Shiltsev and F. Zimmermann, *Rev. Mod. Phys.* **93**, 015006 (2021).
- [3] H. M. Gray, *Reviews in Physics* **6**, 100053 (2021).
- [4] CERN Yellow Reports: Monographs, Vol. 1, “European strategy for particle physics - accelerator r&d roadmap,” (2022).
- [5] T. Roser, R. Brinkmann, S. Cousineau, D. Denisov, S. Gessner, S. Gourlay, P. Lebrun, M. Narain, K. Oide, T. Raubenheimer, J. Seeman, V. Shiltsev, J. Strait, M. Turner, and L.-T. Wang, *Journal of Instrumentation* **18**, P05018 (2023).
- [6] F. Del Gaudio, T. Grismayer, R. A. Fonseca, W. B. Mori, and L. O. Silva, *Phys. Rev. Accel. Beams* **22**, 023402 (2019).
- [7] V. Yakimenko, S. Meuren, F. Del Gaudio, C. Baumann, A. Fedotov, F. Fiuza, T. Grismayer, M. J. Hogan, A. Pukhov, L. O. Silva, and G. White, *Phys. Rev. Lett.* **122**, 190404 (2019).
- [8] W. L. Zhang, T. Grismayer, and L. O. Silva, *Phys. Rev. A* **108**, 042816 (2023).
- [9] M. Tamburini and S. Meuren, *Phys. Rev. D* **104**, L091903 (2021).
- [10] T. Katsouleas, J. J. Su, W. B. Mori, and J. M. Dawson, *Physics of Fluids B: Plasma Physics* **2**, 1384 (1990).
- [11] P. Chen, *Phys. Rev. D* **46**, 1186 (1992).
- [12] T. Barklow, S. Gessner, M. Hogan, C.-K. Ng, M. Peskin, T. Raubenheimer, G. White, E. Adli, G. J. Cao, C. A. Lindström, K. Sjobak, S. Barber, C. Geddes, A. Formenti, R. Lehe, C. Schroeder, D. Terzani, J. van Tilborg, J.-L. Vay, E. Zoni, C. Doss, M. Litos, I. Lobach, J. Power, M. Swiatlowski, L. Fedeli, H. Vincenti, T. Grismayer, M. Vranic, and W. Zhang, *Journal of Instrumentation* **18**, P09022 (2023).
- [13] P. Chen and V. I. Telnov, *Phys. Rev. Lett.* **63**, 1796 (1989).
- [14] P. Chen and K. Yokoya, *Phys. Rev. D* **38**, 987 (1988).
- [15] D. Schulte, in *Proceedings of the CAS-CERN Accelerator School: Intensity Limitations in Particle Beams*, Vol. 3, edited by W. Herr (CERN, Geneva, Switzerland, 2017) pp. 431–445.
- [16] C. B. Schroeder, E. Esarey, C. G. R. Geddes, C. Benedetti, and W. P. Leemans, *Phys. Rev. ST Accel. Beams* **13**, 101301 (2010).
- [17] A. S. Samsonov, E. N. Nerush, I. Y. Kostyukov, M. Filipovic, C. Baumann, and A. Pukhov, *New J. Phys.* **23**, 103040 (2021).
- [18] T. Barklow, C. Emma, Z. Huang, A. Naji, E. Nanni, A. Schwartzman, S. Tantawi, and G. White, “Xcc: an x-ray fel-based  $\gamma\gamma$  collider higgs factory,” (2022), arXiv:2203.08484 [hep-ph].
- [19] W. L. Zhang, T. Grismayer, K. M. Schoeffler, R. A. Fonseca, and L. O. Silva, *Phys. Rev. E* **103**, 013206 (2021).
- [20] K. Qu, S. Meuren, and N. J. Fisch, *Phys. Rev. Lett.* **127**, 095001 (2021).
- [21] T. Grismayer, M. Vranic, J. L. Martins, R. A. Fonseca, and L. O. Silva, *Physics of Plasmas* **23**, 056706 (2016).
- [22] E. N. Nerush, I. Y. Kostyukov, A. M. Fedotov, N. B. Narozhny, N. V. Elkina, and H. Ruhl, *Phys. Rev. Lett.* **106**, 035001 (2011).
- [23] A. Philippov, A. Timokhin, and A. Spitkovsky, *Phys. Rev. Lett.* **124**, 245101 (2020).
- [24] A. N. Timokhin, *Mon. Not. R. Astron. Soc.* **408**, 2092 (2010).
- [25] F. Cruz, T. Grismayer, A. Y. Chen, A. Spitkovsky, and L. O. Silva, *Astrophys. J. Lett.* **919**, L4 (2021).
- [26] V. I. Ritus, *J. Sov. Laser Res.; (United States)* **6** (1985), 10.1007/BF01030001.
- [27] A. Di Piazza, C. Müller, K. Z. Hatsagortsyan, and C. H. Keitel, *Rev. Mod. Phys.* **84**, 1177 (2012).
- [28] A. Gonoskov, T. G. Blackburn, M. Marklund, and S. S. Bulanov, *Rev. Mod. Phys.* **94**, 045001 (2022).
- [29] A. Fedotov, A. Ilderton, F. Karbstein, B. King, D. Seipt, H. Taya, and G. Torgrimsson, *Physics Reports* **1010**, 1 (2023), advances in QED with intense background fields.
- [30] M. Pouyez, T. Grismayer, M. Grech, and C. Riconda, arXiv:2411.03377 (2024).
- [31] M. Pouyez, A. Mironov, T. Grismayer, A. Mercuri-Baron, F. Perez, M. Vranic, C. Riconda, and M. Grech, arXiv:2402.04501 (2024).
- [32] R. A. Fonseca, L. O. Silva, F. S. Tsung, V. K. Decyk, W. Lu, C. Ren, W. B. Mori, S. Deng, S. Lee, T. Katsouleas, and J. C. Adam, in *Computational Science — ICCS 2002*, edited by P. M. A. Sloot, A. G. Hoekstra, C. J. K. Tan, and J. J. Dongarra (Springer Berlin Heidelberg, Berlin, Heidelberg, 2002) pp. 342–351.
- [33] See Supplemental Material [URL] for a description of the SF-QED module implemented in the OSIRIS code, the details of PIC simulations shown in this Letter, the validity analysis of the performed simulations, and the brief comparison of simulation results between OSIRIS and GUINEA-PIG, which includes Refs. [39, 40].
- [34] H. Wiedemann, *Particle Accelerator Physics* (Springer Cham, 2015).
- [35] D. Schulte, *Study of Electromagnetic and Hadronic Background in the Interaction Region of the TESLA Collider*, Ph.D. thesis, University of Hamburg (1996).
- [36] W. Zhang, T. Grismayer, R. Fonseca, and L. Silva, “Disruption-induced kink instability in the leptonic beam collision driven by qed effects, poster presented at the 47th eps conference on plasma physics 2021,”.
- [37] K. Yokoya and P. Chen, in *Frontiers of Particle Beams: Intensity Limitations: Proceedings of a Topical Course Held by the Joint US-CERN School on Particle Acceler-*

ators at Hilton Head Island, South Carolina, USA 7–14 November 1990 (Springer, 2005) pp. 415–445.

[38] D. Del Sorbo, F. Del Gaudio, P. Alves, H. Chu, T. Grismayer, W. Zhang, L. Silva, W. Mori, and F. Fiuza,

“Electron-positron qed cascades in the collision of tightly focused lepton beams,”

[39] J. M. Dawson, *Rev. Mod. Phys.* **55**, 403 (1983).

[40] C. K. Birdsall and A. B. Langdon, *Plasma Physics via Computer Simulation* (CRC Press, 1991).

## Supplemental Material: Anomalous pinch in electron-electron beam collision

W. Zhang,<sup>1,2</sup> \* T. Grismayer,<sup>3</sup> and L. O. Silva<sup>3</sup>

<sup>1</sup>*Jiangxi Province Key Laboratory of Nuclear Physics and Technology  
East China University of Technology, Nanchang 330013, China*

<sup>2</sup>*Engineering Research Center of Nuclear Technology Application,*

*Ministry of Education, East China University of Technology, Nanchang 330013, China*

<sup>3</sup>*GoLP/Instituto de Plasmas e Fusão Nuclear, Instituto Superior Técnico, Universidade de Lisboa, Lisboa, Portugal*

\*Email: wenlong.zhang@ecut.edu.cn

### I. QED-PIC SIMULATIONS

#### A. PIC and SF-QED

Particle-in-cell (PIC) codes are one of the most important research tools in plasma physics [39, 40] as they describe the self-consistent microscopic interaction between a collection of charged particles. The standard loop of the PIC method can be summarized as follows. The simulation domain is represented by a discrete spatial grid, in which macro-particles, representing an ensemble of real particles, move continuously. As they move across the grid, charged macro-particles carry electrical currents deposited on the grid vertices. These currents, defined with the vector  $\mathbf{J}$ , are then used to advance the electric and magnetic fields  $\mathbf{E}$  and  $\mathbf{B}$  in time via Faraday’s and Ampere’s laws. The updated electromagnetic field values, defined on the grid vertices, are then interpolated to the particles’ positions and used to compute the Lorentz force acting on them.

When the plasma is exposed to intense electromagnetic fields, the particle dynamics can enter the strong-field quantum electrodynamics (SF-QED) regime. The SF-QED regime is characterized by the dimensionless parameter  $\chi_e$

$$\chi_e = \frac{1}{E_s} \sqrt{\left(\gamma \mathbf{E} + \frac{\mathbf{p}}{mc} \times \mathbf{B}\right)^2 - \left(\frac{\mathbf{p}}{mc} \cdot \mathbf{E}\right)^2}, \quad (\text{S1})$$

where  $E_s = m^2 c^3 / e \hbar = 4.41 \times 10^{13}$  statV/cm is the Schwinger field with  $e$  and  $m$  are the charge and mass of an electron,  $\hbar$  is the reduced Planck constant,  $c$  is the speed of light in vacuum,  $\gamma$  and  $\mathbf{p}$  are the particle’s Lorentz factor and momentum. When  $\chi_e \gtrsim 1$ , the photon emission is purely quantum and the photons have a non-negligible probability of decaying into an electron-positron pair [28, 29]. The SF-QED regime is reached when the ultra-relativistic dense lepton beams are collided. Modeling these collisions requires being able to describe the SF-QED processes and also the collective beam motion due to the self-fields of the beam.

It is in this way that PIC simulations enriched with a QED module prove to be the ideal tool to study the beam-beam physics at the Interaction Point (IP) of lepton colliders [6, 8, 17]. The PIC method intrinsically ensures a self-consistent calculation for the evolution of beam motion and fields, as well as the quantum radiation and  $e^-e^+$  pair production. This makes PIC simulations a powerful tool for studying beam-beam collisions, especially in the high-disruption and strong-quantum regimes.

#### B. SF-QED processes in OSIRIS

OSIRIS [32] has been extended to incorporate several SF-QED processes, including nonlinear Compton scattering (NCS) also known as the quantum-corrected synchrotron radiation, and nonlinear Breit-Wheeler (NBW) for  $e^-e^+$  pair production. These two phenomena are the leading and most relevant QED processes [28, 29] in strong fields.

NCS is the interaction between a lepton with energy  $\mathcal{E}_0 = \gamma mc^2$  and a background electromagnetic field. In this interaction, the lepton emits a gamma-ray photon with energy  $\mathcal{E}_\gamma = \xi \mathcal{E}_0$ . Under the locally constant field

approximation (LCFA), the differential probability rate of NCS reads

$$\frac{d^2 P_\gamma}{dt d\xi} = \frac{\alpha}{\sqrt{3}\pi\tau_c\gamma} \left[ \int_b^\infty K_{5/3}(q) dq + \frac{\xi^2}{1-\xi} K_{2/3}(b) \right],$$

where  $\tau_c = \hbar/mc^2$  is the Compton time.  $\alpha$  is the fine-structure constant.  $b = 2/(3\chi_e)\xi_\gamma/(1-\xi)$ ,  $K_\nu$  the modified Bessel function of the second kind, and  $\chi_e$  is quantum parameter given by Eq. (S1). The total rate is given by  $dP_\gamma/dt = \int_0^1 (d^2 P_\gamma/dt d\xi) d\xi$ . In the strong-quantum regime ( $\chi_e \gg 1$ ),  $dP_\gamma/dt \simeq 1.46\alpha/(\tau_c\gamma)\chi_e^{2/3}$ .

While the emitted photons propagate in the electromagnetic field, they can decay into an  $e^-e^+$  pair through the NBW process. The differential probability rate of NBW pair production is

$$\frac{d^2 P_{pp}}{dt d\xi^-} = \frac{\alpha mc^2}{\sqrt{3}\pi\tau_c\mathcal{E}_\gamma} \left[ \left( \frac{\xi^+}{\xi^-} + \frac{\xi^-}{\xi^+} \right) K_{2/3}(b) + \int_b^\infty K_{1/3}(q) dq \right],$$

where

$$\xi^- = \frac{\mathcal{E}^-}{\mathcal{E}_\gamma}, \quad \xi^+ = \frac{\mathcal{E}^+}{\mathcal{E}_\gamma}, \quad b = \frac{2}{3\chi_\gamma} \frac{1}{\xi^- \xi^+},$$

with  $\mathcal{E}^-$  and  $\mathcal{E}^+$  being the energies of the produced electron and positron, respectively. The quantum parameter  $\chi_\gamma$  is similarly defined as

$$\chi_\gamma = \frac{1}{E_s} \sqrt{\left( \frac{\mathcal{E}_\gamma}{mc^2} \mathbf{E} + \frac{\hbar \mathbf{k}_\gamma}{mc} \times \mathbf{B} \right)^2 - \left( \frac{\hbar \mathbf{k}_\gamma}{mc} \cdot \mathbf{E} \right)^2}, \quad (\text{S2})$$

where  $\mathbf{k}_\gamma$  is the wave vector of the photon. The quantum parameter of the produced pairs can be obtained as  $\chi_e^\pm = \xi^\pm \chi_\gamma$ . Similarly, the overall rate of pair production is given by  $dP_{pp}/dt = \int_0^1 (d^2 P_{pp}/dt d\xi^-) d\xi^-$ . For the strong-quantum regime ( $\chi_\gamma \gg 1$ ),  $dP_{pp}/dt \simeq 0.38\alpha mc^2/(\tau_c \mathcal{E}_\gamma) \chi_\gamma^{2/3}$ .

Both NCS and NBW are implemented in OSIRIS with a Monte Carlo method. For NCS, at each time step photons are created randomly according to the total rate, and the corresponding energies are sampled according to the differential probability rate. The pair creation follows the same method. The momentum conservation is ensured by subtracting the momentum of the created photon to the lepton. For NBW, the photon is removed from the simulation and its energy is distributed between the new electron and positron.

## II. SIMULATION DETAILS

### A. Simulation parameters

As an illustration, we give the details of the parameters of the simulation shown in Fig. 2. The colliding electron beams are cylinder-shaped with uniform density ( $n_0$ ). The beam parameters are:  $\mathcal{E}_0 = 70$  GeV,  $\sigma_z = 12$   $\mu\text{m}$ ,  $\sigma_0 = 4.9$  nm, and  $N_0 = 1.3 \times 10^9$ , corresponding to  $n_0 = 1.4 \times 10^{24}$   $\text{cm}^{-3}$ ,  $D = 54$ , and  $\chi_{e \text{ max}} = 13$ . The simulation box ( $x, y, z$ ) is  $125 \text{ nm} \times 125 \text{ nm} \times 24 \text{ } \mu\text{m}$  resolved by  $300 \times 300 \times 30000$  grids with spatial resolutions of  $\Delta x = \Delta y = 0.08\sigma_0$  and  $\Delta z = 6.7 \times 10^{-5}\sigma_z$ . We have 4 particles-per-cell (PPC) which corresponds to a total of  $2.6 \times 10^7$  macro-particles per beam. The time step is  $\Delta t = 2.2 \times 10^{-5}\sigma_z/c$ . The simulation lasts until both beams completely cross each other. The time step is chosen such that to resolve both collective beam physics and SF-QED time scales. To carefully model NCS, one has to satisfy  $\Delta t \ll \tau_\gamma = (dP_\gamma/dt)^{-1}$ . Moreover, the collective motion is well resolved if  $\Delta t \ll \tau_D$  where  $\tau_D = D^{-1/2}\sigma_z/c$  is the disruption time-scale.

For simulations shown in Fig. 4, we kept similar resolutions and number of macro-particles as those in Fig. 2. For instance, the simulation with  $D = 122$  (Figure 4(b) and 4(c)) has  $\Delta x = \Delta y = 0.08\sigma_0$ ,  $\Delta z = 3.5 \times 10^{-5}\sigma_z$ , and  $\Delta t = 1.7 \times 10^{-5}\sigma_z/c$ . The computation load and memory usage generally increase with the disruptions. Therefore, for higher disruption, we set 2 PPC, which corresponds to  $2.5 \times 10^7$  macro-particles per beam.

### B. Locally constant field approximation

The differential probability rates used in OSIRIS simulations require that the LCFA remains valid. The condition for valid LCFA in a quantum-dominated beam-beam collision has been derived in Ref. [8], and is given by

$$\left(\frac{\sigma_0}{d_e}\right)^{2/3} \frac{\sigma_z}{d_e} \gg \left(\gamma \frac{\lambda_c}{d_e}\right)^{1/3} \quad (\text{S3})$$

where  $\lambda_c = \hbar/mc = 3.86 \times 10^{-11}$  cm is the reduced Compton length and  $d_e = c/\omega_p$  is the electron skin depth, with  $\omega_p = \sqrt{4\pi n_0 e^2/m}$  the beam plasma frequency. Equation (S3) is always satisfied for all simulations presented in this Letter.

### III. Comparison with GUINEA-PIG

GUINEA-PIG is a widely used, specialized code for studying beam-beam collisions [35]. We have performed GUINEA-PIG simulations with high resolutions in order to benchmark our OSIRIS results. When SF-QED is turned off, GUINEA-PIG gives the same luminosity  $L_0$  as the one computed in our PIC simulations. When SF-QED is turned on, the anomalous pinch is also observed in GUINEA-PIG simulations. The time corresponding to the onset of the pinch  $t_{\text{AP}}$  is measured to be the same in both codes. However, the luminosity recorded in GUINEA-PIG is slightly lower than that in OSIRIS. In addition, we observed that the enhancement of the quantum parameter  $\chi_e$  in OSIRIS is higher than that in GUINEA-PIG. We believe that these differences are due to the resolution of our GUINEA-PIG simulations, since the extreme compression of the beams may be under-resolved as well as the corresponding field amplification. A detailed, systematic comparison between the GUINEA-PIG and OSIRIS simulations will be provided in a future publication.